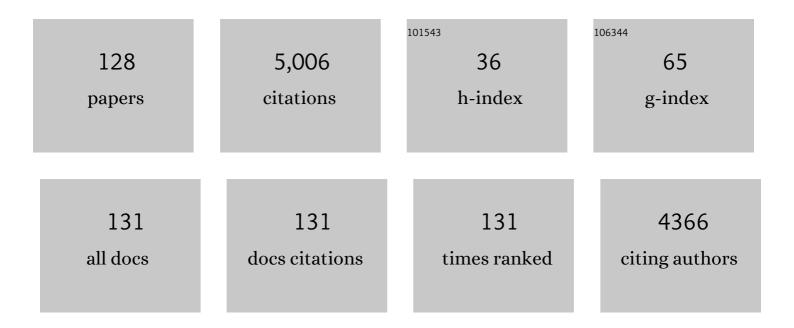
Chris Harris

List of Publications by Year in descending order

Source: https://exaly.com/author-pdf/7343722/publications.pdf Version: 2024-02-01



#	Article	IF	CITATIONS
1	Hydrochemical characteristics of aquifers near Sutherland in the Western Karoo, South Africa. Journal of Hydrology, 2001, 241, 91-103.	5.4	379
2	Magmatic evolution of the Alboran region: The role of subduction in forming the western Mediterranean and causing the Messinian Salinity Crisis. Earth and Planetary Science Letters, 2004, 218, 91-108.	4.4	255
3	Origins of Large Volume Rhyolitic Volcanism in the Antarctic Peninsula and Patagonia by Crustal Melting. Journal of Petrology, 2001, 42, 1043-1065.	2.8	235
4	A role for lower continental crust in flood basalt genesis? Isotopic and incompatible element study of the lower six formations of the western Deccan Traps. Geochimica Et Cosmochimica Acta, 1994, 58, 267-288.	3.9	219
5	Silica alteration zones in the Barberton greenstone belt: A window into subseafloor processes 3.5–3.3ÂGa ago. Chemical Geology, 2008, 257, 221-239.	3.3	157
6	Hydrogen and oxygen isotope geochemistry of Ascension Island lavas and granites: variation with crystal fractionation and interaction with sea water. Contributions To Mineralogy and Petrology, 1985, 91, 74-81.	3.1	111
7	Magmatic origin of giant â€~Kiruna-type' apatite-iron-oxide ores in Central Sweden. Scientific Reports, 2013, 3, 1644.	3.3	110
8	Crustal Contamination and Fluid–Rock Interaction during the Formation of the Platreef, Northern Limb of the Bushveld Complex, South Africa. Journal of Petrology, 2001, 42, 1321-1347.	2.8	105
9	Field Relationships and Geochemical Constraints on the Emplacement of the Jinchuan Intrusion and its Ni-Cu-PGE Sulfide Deposit, Gansu, China. Economic Geology, 2007, 102, 75-94.	3.8	98
10	Oxygen isotope composition of phenocrysts from Tristan da Cunha and Gough Island lavas: variation with fractional crystallization and evidence for assimilation. Contributions To Mineralogy and Petrology, 2000, 138, 164-175.	3.1	97
11	Discriminating between pyroxenite and peridotite sources for continental flood basalts (CFB) in southern Africa using olivine chemistry. Earth and Planetary Science Letters, 2017, 475, 143-151.	4.4	96
12	The Petrology of Lavas and Associated Plutonic Inclusions of Ascension Island. Journal of Petrology, 1983, 24, 424-470.	2.8	95
13	OXYGEN ISOTOPE COMPOSITION OF GARNET IN THE PENINSULA GRANITE, CAPE GRANITE SUITE, SOUTH AFRICA: CONSTRAINTS ON MELTING AND EMPLACEMENT MECHANISMS. South African Journal of Geology, 2010, 113, 401-412.	1.2	85
14	Oxygen and hydrogen isotope geochemistry of S- and I-type granitoids: the Cape Granite suite, South Africa. Chemical Geology, 1997, 143, 95-114.	3.3	82
15	The Petrogenesis of the Kirwan Basalts of Dronning Maud Land, Antarctica. Journal of Petrology, 1990, 31, 341-369.	2.8	76
16	Global Fe–O isotope correlation reveals magmatic origin of Kiruna-type apatite-iron-oxide ores. Nature Communications, 2019, 10, 1712.	12.8	75
17	The origin of low δ18O granites and related rocks from the Seychelles. Contributions To Mineralogy and Petrology, 2002, 143, 366-376.	3.1	73
18	The oxygen isotope composition of Karoo and Etendeka picrites: High δ180 mantle or crustal contamination?. Contributions To Mineralogy and Petrology, 2015, 170, 1.	3.1	73

#	Article	IF	CITATIONS
19	Coupled silicon–oxygen isotope fractionation traces Archaean silicification. Earth and Planetary Science Letters, 2011, 301, 222-230.	4.4	70
20	Petrology of the Alkaline Core of the Messum Igneous Complex, Namibia: Evidence for the Progressively Decreasing Effect of Crustal Contamination. Journal of Petrology, 1999, 40, 1377-1397.	2.8	68
21	The pre-eruptive magma plumbing system of the 2007–2008 dome-forming eruption of Kelut volcano, East Java, Indonesia. Contributions To Mineralogy and Petrology, 2013, 166, 275-308.	3.1	68
22	Oxygen and neodymium isotope evidence for source diversity in Cretaceous anorogenic granites from Namibia and implications for A-type granite genesis. Lithos, 2004, 73, 21-40.	1.4	61
23	The impact of resolving the Rossby radius at mid-latitudes in the ocean: results from a high-resolution version of the Met Office GC2 coupled model. Geoscientific Model Development, 2016, 9, 3655-3670.	3.6	61
24	Low-δ18O silicic magmas on Earth: A review. Earth-Science Reviews, 2020, 208, 103299.	9.1	61
25	O- AND H-ISOTOPE RECORD OF CAPE TOWN RAINFALL FROM 1996 TO 2008, AND ITS APPLICATION TO RECHARGE STUDIES OF TABLE MOUNTAIN GROUNDWATER, SOUTH AFRICA. South African Journal of Geology, 2010, 113, 33-56.	1.2	60
26	The production of large-volume, low-δ18O rhyolites during the rifting of Africa and Antarctica: The Lebombo Monocline, southern Africa. Geochimica Et Cosmochimica Acta, 1992, 56, 3561-3570.	3.9	57
27	Oxygen isotope geochemistry of the Mesozoic anorogenic complexes of Damaraland, northwest Namibia: evidence for crustal contamination and its effect on silica saturation. Contributions To Mineralogy and Petrology, 1995, 122, 308-321.	3.1	57
28	Early Cretaceous Basaltic and Rhyolitic Magmatism in Southern Uruguay Associated with the Opening of the South Atlantic. Journal of Petrology, 2000, 41, 1413-1438.	2.8	56
29	Deposition, Diagenesis, and Secondary Enrichment of Metals in the Paleoproterozoic Hotazel Iron Formation, Kalahari Manganese Field, South Africa. Economic Geology, 2003, 98, 1449-1462.	3.8	54
30	Assimilation of carbonate country rock by the parent magma of the Panzhihua Fe-Ti-V deposit (SW) Tj ETQq0 0	0 rgBT /0\	verlock 10 Tf 5
31	The Tongde dioritic pluton (Sichuan, SW China) and its geotectonic setting: Regional implications of a local-scale study. Gondwana Research, 2010, 18, 455-465.	6.0	49
32	Floating stones off El Hierro, Canary Islands: xenoliths of pre-island sedimentary origin in the early products of the October 2011 eruption. Solid Earth, 2012, 3, 97-110.	2.8	49
33	Magmatic differentiation processes at Merapi Volcano: inclusion petrology and oxygen isotopes. Journal of Volcanology and Geothermal Research, 2013, 261, 38-49.	2.1	49
34	Highâ€resolution geochemical record of fluid–rock interaction in a midâ€crustal shear zone: a comparative study of major element and oxygen isotope transport in garnet. Journal of Metamorphic Geology, 2012, 30, 255-280.	3.4	39
35	Petrogenesis of the Swaziland and Northern Natal Rhyolites of the Lebombo Rifted Volcanic Margin, South East Africa. Journal of Petrology, 2006, 48, 185-218.	2.8	38
36	Stable isotope and 14C study of biogenic calcrete in a termite mound, Western Cape, South Africa, and	1.7	37

its palaeoenvironmental significance. Quaternary Research, 2009, 72, 258-264.

#	Article	IF	CITATIONS
37	Skarn xenolith record crustal CO2 liberation during Pompeii and Pollena eruptions, Vesuvius volcanic system, central Italy. Chemical Geology, 2015, 415, 17-36.	3.3	37
38	Discordant ultramafic pegmatoidal pipes in the Bushveld Complex. Contributions To Mineralogy and Petrology, 2000, 140, 119-133.	3.1	36
39	Low-temperature hydrothermal alteration of intra-caldera tuffs, Miocene Tejeda caldera, Gran Canaria, Canary Islands. Journal of Volcanology and Geothermal Research, 2008, 176, 551-564.	2.1	36
40	O-isotope Study of the Bushveld Complex Granites and Granophyres: Constraints on Source Composition, and Assimilation. Journal of Petrology, 2011, 52, 2221-2242.	2.8	36
41	Magma reservoir dynamics at Toba caldera, Indonesia, recorded by oxygen isotope zoning in quartz. Scientific Reports, 2017, 7, 40624.	3.3	36
42	Isotopic composition of lead and strontium in lavas and coarse-grained blocks from Ascension Island, South Atlantic. Earth and Planetary Science Letters, 1982, 60, 79-85.	4.4	35
43	Oxygen isotope geochemistry of the silicic volcanic rocks of the Etendeka-ParanÃ; province: Source constraints. Geology, 1990, 18, 1119.	4.4	35
44	Re and Os distribution and Os isotope composition of the Platreef at the Sandsloot–Mogolakwena mine, Bushveld complex, South Africa. Chemical Geology, 2011, 281, 352-363.	3.3	35
45	Relationship between footwall composition, crustal contamination, and fluid–rock interaction in the Platreef, Bushveld Complex, South Africa. Mineralium Deposita, 2008, 43, 825-848.	4.1	34
46	Origins of strandline duricrusts around the Makgadikgadi Pans (Botswana Kalahari) as deduced from their chemical and isotope composition. Sedimentary Geology, 2009, 219, 262-279.	2.1	34
47	Tectonic significance and redox state of Paleoproterozoic eclogite and pyroxenite components in the Slave cratonic mantle lithosphere, Voyageur kimberlite, Arctic Canada. Chemical Geology, 2017, 455, 98-119.	3.3	33
48	Geology and petrogenesis of the Straumsvola nepheline syenite complex, Dronning Maud Land, Antarctica. Geological Magazine, 1993, 130, 513-532.	1.5	32
49	Fluid inclusion and stable isotope (O, H, C, and S) constraints on the genesis of the Serrinha gold deposit, Gurupi Belt, northern Brazil. Mineralium Deposita, 2006, 41, 160-178.	4.1	31
50	Origin of garnet in aplite and pegmatite from Khajeh Morad in northeastern Iran: A major, trace element, and oxygen isotope approach. Lithos, 2014, 208-209, 378-392.	1.4	31
51	Small-scale Sr and O isotope variations through the UG2 in the eastern Bushveld Complex: The role of crustal fluids. Chemical Geology, 2018, 485, 100-112.	3.3	31
52	Geochemistry of the Mesozoic regional basic dykes of western Dronning Maud Land, Antarctica. Contributions To Mineralogy and Petrology, 1991, 107, 100-111.	3.1	30
53	Oxygen and hydrogen isotope composition of kaolinite deposits, Cape Peninsula, South Africa; low-temperature, meteoric origin. Economic Geology, 1999, 94, 1353-1366.	3.8	30
54	Stable isotope and fluid inclusion evidence for the origin of the Brandberg West area Sn–W vein deposits, NW Namibia. Mineralium Deposita, 2006, 41, 671-690.	4.1	28

#	Article	IF	CITATIONS
55	Geology and Fluid Characteristics of the Mina Velha and Mandiocal Orebodies and Implications for the Genesis of the Orogenic Chega Tudo Gold Deposit, Gurupi Belt, Brazil. Economic Geology, 2008, 103, 957-980.	3.8	28
56	Pyroxene standards for SIMS oxygen isotope analysis and their application to Merapi volcano, Sunda arc, Indonesia. Chemical Geology, 2016, 447, 1-10.	3.3	27
57	Quartz vein formation by local dehydration embrittlement along the deep, tremorgenic subduction thrust interface. Geology, 2018, 46, 67-70.	4.4	27
58	The age and country rock provenance of the Molopo Farms Complex: implications for Transvaal Supergroup correlation in southern Africa. South African Journal of Geology, 2019, 122, 39-56.	1.2	25
59	A Quantitative Study of Magmatic Inclusions in the Plutonic Ejecta of Ascension Island. Journal of Petrology, 1986, 27, 251-276.	2.8	24
60	Stable isotope study of the Archaean rocks of the Vredefort impact structure, central Kaapvaal Craton, South Africa. Contributions To Mineralogy and Petrology, 2007, 155, 63-78.	3.1	24
61	Helium isotope evidence for a deep-seated mantle plume involved in South Atlantic breakup. Geology, 2017, 45, 827-830.	4.4	24
62	Multi-level magma plumbing at Agung and Batur volcanoes increases risk of hazardous eruptions. Scientific Reports, 2018, 8, 10547.	3.3	24
63	Combined igneous and hydrothermal source for the Kiruna-type Bafq magnetite-apatite deposit in Central Iran; trace element and oxygen isotope studies of magnetite. Ore Geology Reviews, 2019, 105, 590-604.	2.7	24
64	Natural partial melting of syenite blocks from Ascension Island. Contributions To Mineralogy and Petrology, 1982, 79, 107-113.	3.1	23
65	Magma plumbing for the 2014–2015 Holuhraun eruption, Iceland. Geochemistry, Geophysics, Geosystems, 2016, 17, 2953-2968.	2.5	22
66	Post-caldera Volcanism at the Heise Volcanic Field: Implications for Petrogenetic Models. Journal of Petrology, 2017, 58, 115-136.	2.8	22
67	Geology and stable isotope (O, H, C, S) constraints on the genesis of the Cachoeira gold deposit, Gurupi Belt, northern Brazil. Chemical Geology, 2005, 221, 188-206.	3.3	21
68	Fluid-Rock Interaction in the Miocene, Post-Caldera, Tejeda Intrusive Complex, Gran Canaria (Canary) Tj ETQq0 0 2149-2176.	0 rgBT 2.8	/Overlock 10 Tf 21
69	Unique chemistry of a diamond-bearing pebble from the Libyan Desert Glass strewnfield, SW Egypt: Evidence for a shocked comet fragment. Earth and Planetary Science Letters, 2013, 382, 21-31.	4.4	21
70	The effect of prior hydrothermal alteration on the melting behaviour during rhyolite formation in Yellowstone, and its importance in the generation of low-1́18O magmas. Earth and Planetary Science Letters, 2018, 481, 338-349.	4.4	21
71	Role of fluids in the metamorphism of the Alpine Fault Zone, New Zealand. Journal of Metamorphic Geology, 2001, 19, 21-31.	3.4	20
72	Pleistocene Dolomite from the Namibian Shelf: High 87Sr/86Sr and Â18O Values Indicate an Evaporative, Mixed-Water Origin. Journal of Sedimentary Research, 2001, 71, 800-808.	1.6	20

#	Article	IF	CITATIONS
73	Temporal evolution of a long-lived syenitic centre: The Kangerlussuaq Alkaline Complex, East Greenland. Lithos, 2006, 92, 276-299.	1.4	20
74	Mafic dykes intrusive into Pre-Cambrian rocks of the São LuÃs cratonic fragment and Gurupi Belt (ParnaÃba Province), north–northeastern Brazil: Geochemistry, Sr–Nd–Pb–O isotopes, 40Ar/39Ar geochronology, and relationships to CAMP magmatism. Lithos, 2013, 172-173, 222-242.	1.4	20
75	An occurrence of rare-earth-rich eudialyte from Ascension Island, South Atlantic. Mineralogical Magazine, 1982, 46, 421-425.	1.4	20
76	Oxygen isotope geochemistry of the Mesozoic volcanics of the Etendeka Formation, Namibia. Contributions To Mineralogy and Petrology, 1989, 102, 454-461.	3.1	19
77	Crustal versus source processes recorded in dykes from the Northeast volcanic rift zone of Tenerife, Canary Islands. Chemical Geology, 2012, 334, 324-344.	3.3	19
78	Magmatic evolution of the Cadamosto Seamount, Cape Verde: beyond the spatial extent of EM1. Contributions To Mineralogy and Petrology, 2012, 163, 949-965.	3.1	19
79	Constraints on Archean crust recycling and the origin of mantle redox variability from the Î′44/40Ca – Î′180 – fO2 signatures of cratonic eclogites. Earth and Planetary Science Letters, 2021, 556, 116720.	4.4	19
80	Hidden mechanical weaknesses within lava domes provided by buried high-porosity hydrothermal alteration zones. Scientific Reports, 2022, 12, 3202.	3.3	19
81	The Cipoeiro gold deposit, Gurupi Belt, Brazil: Geology, chlorite geochemistry, and stable isotope study. Journal of South American Earth Sciences, 2007, 23, 242-255.	1.4	18
82	GEOCHEMICAL PERSPECTIVE ON ORIGINS AND CONSEQUENCES OF HEUWELTJIE FORMATION IN THE SOUTHWESTERN CAPE, SOUTH AFRICA. South African Journal of Geology, 2012, 115, 577-588.	1.2	18
83	Subduction relics in the subcontinental lithospheric mantle evidence from variation in the δ18O value of eclogite xenoliths from the Kaapvaal craton. Contributions To Mineralogy and Petrology, 2019, 174, 1.	3.1	18
84	Magmatic garnet in the Triassic (215 Ma) Dehnow pluton of NE Iran and its petrogenetic significance. International Geology Review, 2014, 56, 596-621.	2.1	17
85	Covariance of initial 87Sr/86Sr ratios, δ18O, and SiO2 in continental flood basalt suites: The role of contamination and alteration. Geology, 1989, 17, 634.	4.4	16
86	Oxygen and carbon isotope geochemistry of the 3.2 Ga Kaap Valley tonalite, Barberton greenstone belt, South Africa. Precambrian Research, 1991, 52, 301-319.	2.7	15
87	Fluid inclusion analysis of silicified Palaeoarchaean oceanic crust – A record of Archaean seawater?. Precambrian Research, 2015, 266, 150-164.	2.7	15
88	Petrogenesis of peralkaline granite dykes of the Straumsvola complex, western Dronning Maud Land, Antarctica. Contributions To Mineralogy and Petrology, 2018, 173, 1.	3.1	14
89	Constraining the sub-arc, parental magma composition for the giant Altiplano-Puna Volcanic Complex, northern Chile. Scientific Reports, 2020, 10, 6864.	3.3	14
90	Sunda arc mantle source δ180 value revealed by intracrystal isotope analysis. Nature Communications, 2021, 12, 3930.	12.8	14

#	Article	IF	CITATIONS
91	Petrogenesis of the Mesozoic Sistefjell syenite intrusion, Dronning Maud Land, Antarctica and surrounding low-Â18O lavas. South African Journal of Geology, 2002, 105, 205-226.	1.2	13
92	Interaction between high-temperature magmatic fluids and limestone explains â€~BastnÃ&type' REE deposits in central Sweden. Scientific Reports, 2019, 9, 15203.	3.3	13
93	Crustal versus mantle origin of carbonate xenoliths from Kimberley region kimberlites using C-O-Sr-Nd-Pb isotopes and trace element abundances. Geochimica Et Cosmochimica Acta, 2019, 266, 258-273.	3.9	13
94	Elemental and B-O-H isotopic compositions of tourmaline and associated minerals in biotite-muscovite granite of Mashhad, NE Iran: Constraints on tourmaline genesis and element partitioning. Lithos, 2019, 324-325, 803-820.	1.4	13
95	Magmatic stoping during the caldera-forming Pomici di Base eruption (Somma-Vesuvius, Italy) as a fuel of eruption explosivity. Lithos, 2020, 370-371, 105628.	1.4	13
96	Structural controls of fluid flow and gold mineralization in the easternmost parts of the Karagwe-Ankole Belt of north-western Tanzania. Ore Geology Reviews, 2016, 77, 332-349.	2.7	12
97	Element and Sr–O isotope redistribution across a plate boundary-scale crustal serpentinite mélange shear zone, and implications for the slab-mantle interface. Earth and Planetary Science Letters, 2019, 522, 198-209.	4.4	12
98	Oxygen isotope evidence for extensive crustal contamination in the Okenyenya igneous complex, Namibia. Geochimica Et Cosmochimica Acta, 1996, 60, 4497-4508.	3.9	11
99	Guano-derived rare earth-rich phosphatic amygdales in gabbroic inclusions from Ascension Island. Earth and Planetary Science Letters, 1985, 72, 141-148.	4.4	9
100	A Mantle-derived Origin for Mauritian Trachytes. Journal of Petrology, 0, , egw052.	2.8	9
101	Hydrogen and oxygen isotope composition of precipitation and stream water on sub-Antarctic Marion Island. Antarctic Science, 2018, 30, 83-92.	0.9	8
102	The role of crustal contamination in the petrogenesis of nepheline syenite to granite magmas in the DitrÄfu Complex, Romania: evidence from O-, Nd-, Sr- and Pb-isotopes. Contributions To Mineralogy and Petrology, 2020, 175, 1.	3.1	8
103	Experimental Melting of Hydrothermally Altered Rocks: Constraints for the Generation of Low-δ18O Rhyolites in the Central Snake River Plain. Journal of Petrology, 2019, 60, 1881-1902.	2.8	7
104	H2O-fluxed melting of eclogite during exhumation: an example from the eclogite type-locality, Eastern Alps (Austria). Lithos, 2021, 390-391, 106118.	1.4	7
105	Formation of low-δ18O magmas of the Kangerlussuaq Intrusion by addition of water derived from dehydration of foundered basaltic roof rocks. Contributions To Mineralogy and Petrology, 2015, 169, 1.	3.1	6
106	Exceptionally high whole-rock δ ¹⁸ 0 values in intra-caldera rhyolites from Northeast Iceland. Mineralogical Magazine, 2018, 82, 1147-1168.	1.4	6
107	Fluid inclusion and stable isotope (O, H, C) constraints on the genesis of the Pedra Branca gold deposit, Troia Massif, Borborema Province, NE Brazil: An example of hypozonal orogenic gold mineralization. Ore Geology Reviews, 2019, 107, 476-500.	2.7	6
108	Stable isotope constraints on the fluid source of hydrothermal breccia pipes in the Tankwa Karoo depocentre, South Africa: Breakdown of authigenic minerals during sill intrusion. Basin Research, 2019, 31, 114-135.	2.7	6

#	Article	IF	CITATIONS
109	Petrogenesis of low-δ18O quartz porphyry dykes, Koegel Fontein complex, South Africa. Contributions To Mineralogy and Petrology, 2018, 173, 1.	3.1	5
110	A large explosive silicic eruption in the British Palaeogene Igneous Province. Scientific Reports, 2019, 9, 494.	3.3	5
111	Whole-rock oxygen isotope ratios as a proxy for the strength and stiffness of hydrothermally altered volcanic rocks. Bulletin of Volcanology, 2022, 84, .	3.0	5
112	Magma and fluid evolution in the lavas and associated granite xenoliths of Ascension Island. Geological Society Special Publication, 1987, 30, 269-272.	1.3	4
113	Reconnaissance Stable Isotope (C, O, H, S) Study of Paleoproterozoic Gold Deposits of the São Luis Craton and Country Rocks, Northern Brazil: Implications for Gold Metallogeny. International Geology Review, 2005, 47, 1131-1143.	2.1	4
114	A low-δ18O intrusive breccia from Koegel Fontein, South Africa: Remobilisation of basement that was hydrothermally altered during global glaciation?. Lithos, 2018, 300-301, 33-50.	1.4	4
115	Dérives de la composition isotopique annuelle des isotopes de O et H comme mesure de la recharge: le cas des sources de la Montagne de la table, Cape Town, Afrique du Sud. Hydrogeology Journal, 2019, 27, 2993-3008.	2.1	4
116	The effects of early Cambrian metamorphism in western Dronning Maud Land, East Antarctica: a carbon and oxygen isotope study of fluid-rock interaction in the Sverdrupfjella Group. Geological Society Special Publication, 2001, 184, 381-394.	1.3	3
117	Microthermometric and O―and Hâ€isotope characteristics of the mineralizing fluid in the AkgÃ1⁄4ney copper–lead–zinc deposit, NE Turkey. International Geology Review, 2009, 51, 375-387.	2.1	3
118	Mineralogical and geochemical criteria to identify the origin and the depositional environment of the upper Numidian babouchite siliceous rocks, northwestern Tunisia. Journal of African Earth Sciences, 2019, 149, 487-502.	2.0	3
119	Absence of hydrothermal oxygen isotope variations in host rocks supports magmatic origin of the giant GrA¤gesberg iron oxide–apatite (IOA) deposit, Central Sweden. International Journal of Earth Sciences, 2022, 111, 425-437.	1.8	3
120	Post-Impact Faulting of the Holfontein Granophyre Dike of the Vredefort Impact Structure, South Africa, Inferred from Remote Sensing, Geophysics, and Geochemistry. Geosciences (Switzerland), 2021, 11, 96.	2.2	2
121	The Garies wollastonite deposit, Namaqualand, South Africa: High-Temperature metamorphism of a low-δ180 skarn?. Canadian Mineralogist, 2021, 59, 495-510.	1.0	2
122	Pre-Teide Volcanic Activity on the Northeast Volcanic Rift Zone. Active Volcanoes of the World, 2013, , 75-92.	1.4	2
123	Stable isotope (O, H and S) studies on the vein-type Cu–Mo–Au mineralization in Qarachilar area, Qaradagh pluton (NW Iran). Neues Jahrbuch Fur Mineralogie, Abhandlungen, 2016, 193, 283-294.	0.3	1
124	lsotopic constraints on fluid evolution and ore precipitation in a sediment-hosted Pb-Ag-Ba-Zn-Cu-Au deposit in the Capricorn Orogen, Western Australia. Applied Geochemistry, 2018, 96, 217-232.	3.0	1
125	Deep infiltration of surface water during deformation? Evidence from a low- δ180 shear zone at Koegel Fontein, Namaqualand, South Africa. Lithos, 2020, 366-367, 105562.	1.4	1
126	Oxygen and hydrogen isotope analysis of experimentally generated magmatic and metamorphic aqueous fluids using laser spectroscopy (WS-CRDS). Chemical Geology, 2021, 584, 120487.	3.3	1

#	Article	IF	CITATIONS
127	Fluid inclusion and isotope (O, H, C, Sr) constraints on the orogenic gold mineralization at the Enche Concha and Tunel prospects, Gurupi Belt, Brazil. Journal of the Geological Survey of Brazil, 2020, 3, 71-84.	0.2	1
128	Petrogenesis of ultramafic rocks of komatiitic composition from the Central Zone of the Limpopo Belt, South Africa: Evidence from O and H isotopes. Journal of African Earth Sciences, 2018, 147, 68-77.	2.0	0